© 2020. Published by The Company of Biologists Ltd | Development (2020) 147, dev193714. doi:10.1242/dev.193714

STEM CELLS AND REGENERATION

RESEARCH ARTICLE

Regeneration in the sponge *Sycon ciliatum* partly mimics postlarval development

Anael Soubigou[1,2], Ethan G. Ross[2,3], Yousef Touhami[2], Nathan Chrismas[2] and Vengamanaidu Modepalli[2,*]

ABSTRACT

Somatic cells dissociated from an adult sponge can reorganize and develop into a juvenile-like sponge, a remarkable phenomenon of regeneration. However, the extent to which regeneration recapitulates embryonic developmental pathways has remained enigmatic. We have standardized and established a sponge *Sycon ciliatum* regeneration protocol from dissociated cells. Morphological analysis demonstrated that dissociated sponge cells follow a series of morphological events resembling postembryonic development. We performed high-throughput sequencing on regenerating samples and compared the data with that from regular postlarval development. Our comparative transcriptomic analysis revealed that sponge regeneration is as equally dynamic as embryogenesis. We found that sponge regeneration is orchestrated by recruiting pathways similar to those utilized in embryonic development. We also demonstrated that sponge regeneration is accompanied by cell death at early stages, revealing the importance of apoptosis in remodelling the primmorphs to initiate re-development. Because sponges are likely to be the first branch of extant multicellular animals, we suggest that this system can be explored to study the genetic features underlying the evolution of multicellularity and regeneration.

KEY WORDS: Development, Evolution, Multicellularity, Regeneration, *Sycon ciliatum*

INTRODUCTION

The regenerative capacity widely varies in the animal kingdom and the sponges are exceptional model organisms with an extraordinary regenerative ability. Anatomical plasticity and cell differentiation is a characteristic feature of sponges, and many sponge cells are capable of transdifferentiation (Ereskovsky, 2010; Adamska, 2018). Dissociated cells from an adult sponge have the unique ability to re-aggregate and fully reconstitute into a functional sponge (Wilson, 1907; Huxley, 1921; Korotkova, 1972). Despite its significance, we still lack an in-depth understanding of the molecular mechanisms and cellular basis of sponge regeneration. Sponges are the ancient extant branch of metazoans (branching order is still debated) (Brunet and King, 2017) and understanding their cellular behaviour during regeneration can provide insights into the evolution of multicellularity. Calcareous sponges have been extensively studied in the past centuries and analysis of their development has significantly influenced evolutionary theory. Terms such as gastrulation were first coined for syconoid species in the classic Calcaronea studies (Haeckel, 1874). *Sycon ciliatum*, a calcareous sponge, is widely explored in embryonic and regeneration studies (Huxley, 1921; Fortunato et al., 2012, 2014a; Leininger et al., 2014; Franzen, 1988).

In *S. ciliatum*, reproduction is viviparous. In brief, after fertilization the embryos develop into a rhomboid shape through early cleavages. Subsequent cell divisions result in the formation of a cup-shaped embryo (stomoblastula). After inversion, the cilia are positioned on the outer surface of the larva and, eventually, the ciliated amphiblastula larva migrates into the radial chamber and swims out of its parent (Fig. 1) (Leininger et al., 2014; Franzen, 1988; Eerkes-Medrano and Leys, 2006). The amphiblastula larva is composed of a single layer of embryonic cells: ciliated micromeres on the anterior pole and non-ciliated granular macromeres on the posterior pole. During metamorphosis, the ciliated cells of the anterior half undergo an epithelial-to-mesenchymal transition and form the inner cell mass; the choanocytes differentiate from these cells. The macromeres envelop the inner cell mass and gradually transform into pinacocytes (pinacoderm). After 24 h following settlement, the spicules (monaxons) are produced by sclerocytes that have differentiated from the inner cell mass. A choanocyte chamber is formed in the inner cell mass and develops into the choanoderm. An osculum is formed at the apical end and the juvenile is elongated along the apical-basal axis, rising into a syconoid body plan (Leininger et al., 2014; Franzen, 1988) (Fig. 1).

Many studies have been dedicated to sponge regeneration in order to understand their morphological signatures, starting from the pioneers of this topic (Wilson, 1907; Huxley, 1921; Huxley and Bourne, 1911). Despite the strong morphological resemblance of sponge regeneration to embryonic and postlarval development (PLD), no study has yet systematically compared them. Several transcriptome studies of regeneration in cnidarians and bilaterians have demonstrated that many developmental pathways are recruited in regeneration (Onai et al., 2007; Amiel et al., 2015; Bryant et al., 2017; Burton and Finnerty, 2009). Hence, we aim to study the regeneration of *S. ciliatum* and compare it with PLD at both morphological and transcriptional levels. We first carried out *S. ciliatum* regeneration to acquire morphological data for comparison with regular PLD and classified the regeneration into seven key stages. Then, we collected the regenerating aggregates at defined time points and performed high-throughput sequencing to compare the transcriptional profiles with those of PLD.

RESULTS AND DISCUSSION

S. ciliatum regeneration morphologically resembles postlarval development

First, we standardized and established a *S. ciliatum* regeneration protocol to achieve consistent sponge regeneration from dissociated cells. Dissociated cells sink to the bottom of the dishes within 1 h of

[1]Sorbonne University, Faculté de Sciences et Ingénierie, Campus Pierre et Marie Curie Jussieu, Paris 75252, France. [2]Marine Biological Association of the UK, The Laboratory, Citadel Hill, Plymouth PL1 2PB, UK. [3]University of Southampton, School of Ocean and Earth Science, Southampton SO17 1BJ, UK.

*Author for correspondence (venmod@mba.ac.uk)

A.S., 0000-0002-8309-5353; V.M., 0000-0003-3099-4969

Handling Editor: Cassandra Extavour
Received 6 June 2020; Accepted 13 October 2020

Development (2020) 147, dev193714. doi:10.1242/dev.193714

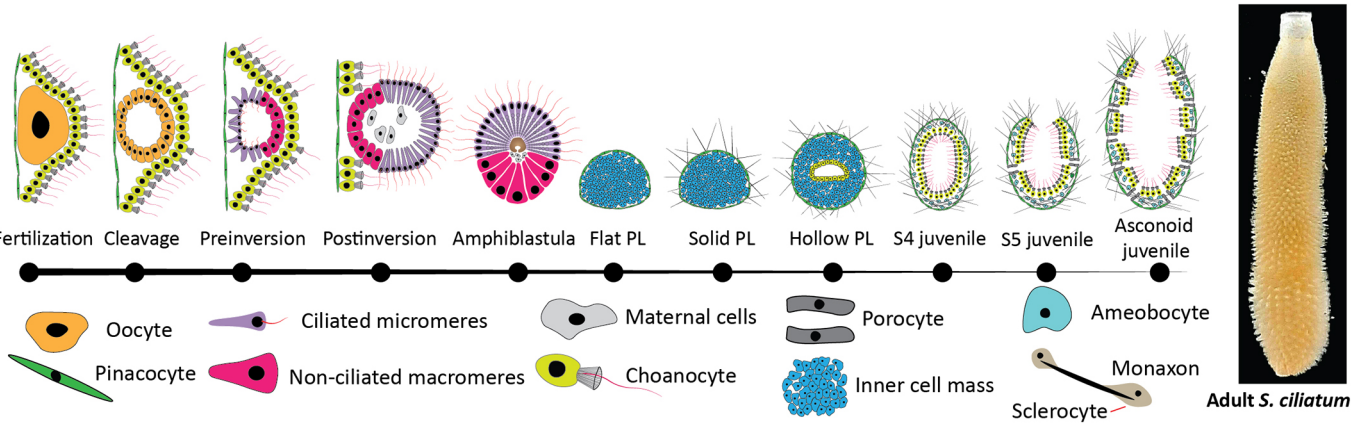

Fig. 1. Representation of embryonic and postlarval development stages in *S. ciliatum*. From left to right: oocyte, cleavage, pre-inversion, post-inversion, amphiblastula (swimming larva), flat post larva, solid post larva, hollow post larvae, choanocyte chamber and asconoid juvenile.

dissociation. Among these cells, we detected choanocytes, amoeboid cells, pieces of spicules and round cells. The majority of cells lose their cell morphology. At 4-6 hours post dissociation (hpd), loose multicellular aggregates of diverse shapes (~10 µm) are formed; these are known as primmorphs. The contacts between cells were not strong and the aggregates fell apart into separated cells upon shaking. Within 24 hpd, these primmorphs significantly increased in size (~100 µm), predominantly as a result of incorporation of cells from suspension or by fusing with other aggregates (Fig. 2A-C). The primmorphs had no defined surface epithelium: pinacocytes and amoebocytes, as well as flagella and collars of choanocytes, were noticeable on the surface, and similar types of cells were found inside the primmorphs (Movies 1-3). During the early stages, cells were actively reorganized and at 48 hpd most cells had lost their typical features, primarily because of transdifferentiation (Fig. 2J-K). The primmorphs became denser and spherical, and two layers of cell types could be identified: a uniform single-cell layer of pinacocytes on the surface and loosely packed granular cells inside the primmorphs (Fig. 2D-F; Movie 3). Earlier studies coined this phenomenon of formation of two distinctive cell layers (the inner cell mass surrounded by a single layer of outer cells) as redevelopment or somatic development (Korotkova, 1972, 1970). Choanocytes on the surface were oriented with their flagella outwards and retained their characteristic features up to 2-3 days post dissociation (dpd); after that, they gradually started losing their typical features (flagellum and microvilli), becoming indistinguishable from other cells (Fig. 2I,L). Largely, two types of primmorphs were observed in the culture: a granulated cell-packed spheroid with a small bubble, and a large bubble with a small inner cell mass (Fig. S1) (termed 'blow-outs' by Huxley, 1921). The latter had an interesting morphology that resembled a blastula with blastocoel. Eventually, a single continuous cavity was formed between the external single cell layer of pinacocytes and internal cell mass (Fig. 2H). At 3 dpd, the primmorphs were entirely covered with pinacocytes, which may possibly have formed through transdifferentiation from choanocytes (Fig. 2J-L).

Around 5 dpd, spicules started appearing from the primmorphs and, simultaneously, multiple ciliated chambers started appearing inside the cell mass. Similar to regular PLD (Leininger et al., 2014), the monaxons were formed first (Fig. 3A,D). Over the next 6-10 days, the ciliated chambers expanded and became lined with choanocyte epithelium (Fig. 3G-I; Movies 4, 5). Gradually, these choanocyte chambers fused into a single epithelial cell layer of choanocytes (also known as choanoderm). At around 16 dpd, a single extended cavity (spongocoel) with osculum formed at the apical end and, simultaneously, multiple porocytes with ostia were formed (Fig. 4A,C; Movie 6). These juveniles continued to elongate along the apical-basal axis, and long straight spicules formed a crown around the osculum. In this study, we maintained the asconoid juveniles for only 3-4 weeks and during this period we observed an increase in the size of spongocoel and number of porocytes with ostia (Fig. 4E-J; Movie 7).

Regeneration in *S. ciliatum* displays a multitude of complex morphogenesis steps, progressing through a series of aggregation, organization and somatic-development events. Based on our current observations and multiple pieces of evidence from previous studies (Wilson, 1907; Huxley, 1921; Korotkova, 1972), we classified sponge regeneration into seven stages based on the morphological and cellular events: (I) aggregation, (II) primmorphs, (III) primmorphs with monaxons, (IV) primmorphs with ciliated chambers, (V) choanoderm, (VI) pre-juvenile (ascon stage) and (VII) juvenile; the details are presented in Table S1 (third column). Remarkably, these morphological signatures were vastly comparable to postembryonic development of *S. ciliatum* (Fig. 1; Table S1, fourth column) (Ereskovsky, 2010; Fortunato et al., 2014a). To gain further insights into their morphological overlap, we compared regeneration with postembryonic development. The embryogenesis of calcaronean sponges has been well described at light and electron microscopy levels (Ereskovsky, 2010; Leininger et al., 2014; Eerkes-Medrano and Leys, 2006). Our morphological comparison was performed using the data from published *S. ciliatum* postembryonic development studies (Leininger et al., 2014). As demonstrated in Table S1, apart from the initial stages of primmorphs at days 1, 2 and 3, the majority of *S. ciliatum* regeneration steps overlap with normal *S. ciliatum* development directly after metamorphosis, including developmental stages S2, S3, S4, S5 and YS (Leininger et al., 2014).

The gene expression of regenerating *S. ciliatum* is as dynamic as postlarval development

A long-standing question in the field of sponge regeneration is whether and to what degree regeneration recapitulates embryonic developmental pathways. Extensive morphological similarities between regeneration and PLD have driven us to explore the gene expression pattern of both processes. We sequenced regenerating

Development (2020) 147, dev193714. doi:10.1242/dev.193714

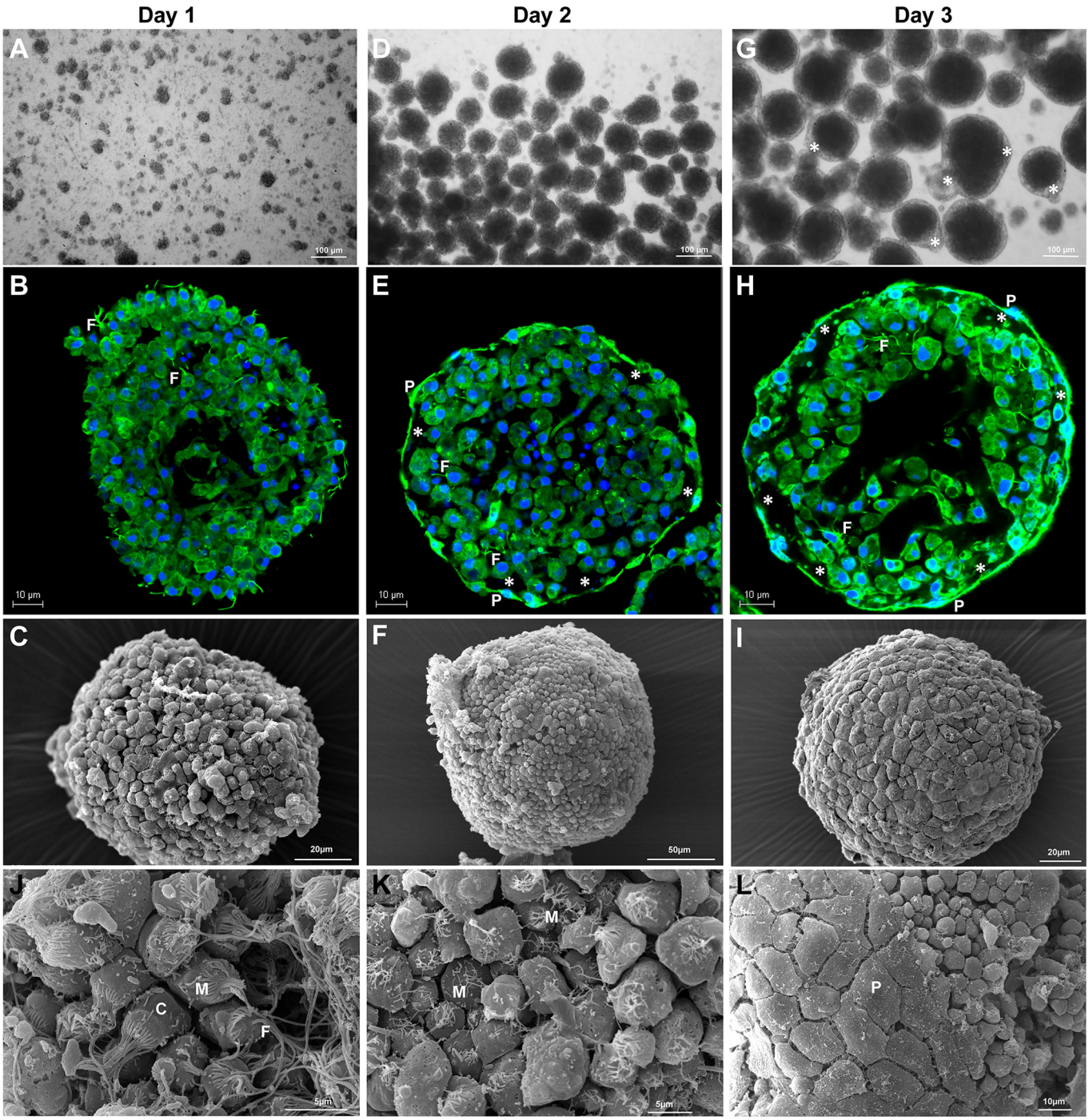

Fig. 2. Morphological and cellular events during the primmorph stage. Regeneration proceeds with the aggregation of dissociated cells and transformation of the loosely connected external cells into an intact single layer of pinacocytes. (A-C) Initial multicellular aggregates in the culture (24 hpd), with loosely aggregated primmorphs. The primmorphs have no defined surface epithelium and are made of diverse cell types. (D) General view of primmorphs in culture after 2 dpd. (E,F) An intact single layer of cells surrounds primmorphs, separating from the inner cell mass, similar to a blastocyst. (G) General view of primmorphs in culture after 3 dpd. (H,I) The external ameboid or cuboidal cells are transformed into flat pinacocytes. The external cavity (*) resembles the extraembryonic cavity with a single layer of flat cells. (E,F,H,I) Fusion of the external cells surrounding the primmorphs, accompanied by transdifferentiation of the choanocytes and other external ameboid cells. (J-L) Choanocyte transdifferentiation into pinacocytes, showing choanocytes with intact flagella and microvilli at 1 dpd (J). Gradually these morphological features are lost through transdifferentiation and a layer of flat pinacocytes is formed (K,L). Images were taken with a bright field (A,D,G), confocal (B,E,H) or scanning electron microscopy (SEM) (C,F,I) microscope. Anti-α-tubulin (green) staining with the nuclei counterstained with DAPI (blue). C, choanocytes; F, flagella; M, microvilli; P, pinacocyte; *, external cavity.

samples at seven time points spanning from day 1 to day 24 after dissociation, including 1, 2, 3-4, 6-8, 10-14, 16-18 (PJUV) and 21-24 (JUV) dpd. For PLD, the RNA sequencing (RNA-seq) datasets spanning seven time points were collected from previously published data (deposited in ENA under accession numbers PRJEB7138 and PRJEB5970) including amphiblastula (swimming larva), flat post larva (S1), solid post larva (S2), hollow post larvae (S3), S4 juvenile, S5 juvenile and asconoid

Development (2020) 147, dev193714. doi:10.1242/dev.193714

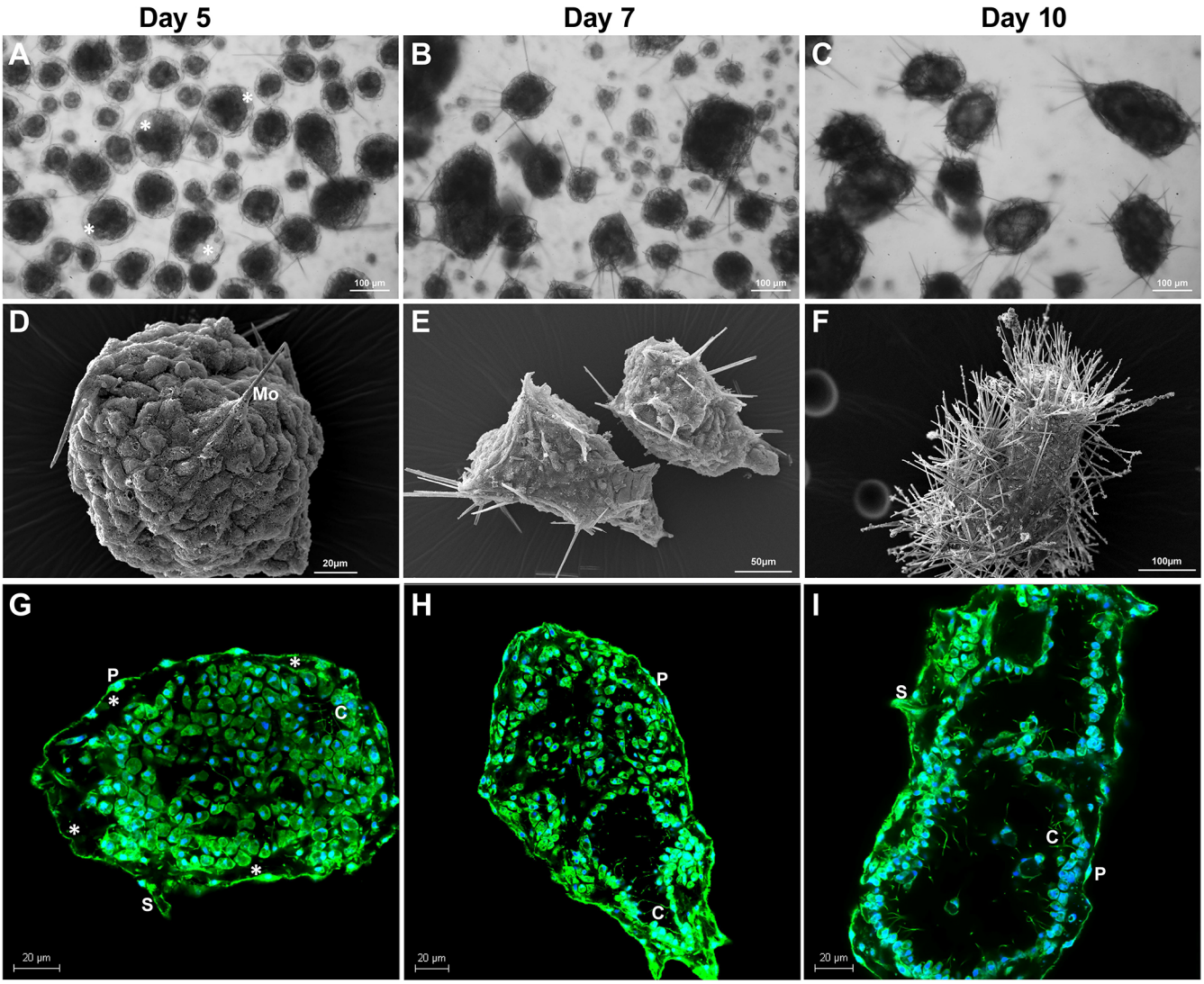

Fig. 3. Specule formation during regeneration. (A-C) General view of primmorphs developing spicules (4-10 dpd). (D,G) Primmorphs develop multiple chambers surrounded by ciliated cells and simultaneously the spicules start appearing as monaxons. (D-F) The gradual increase in the number of spicules. (G-I) Expansion and integration of choanocyte chambers and eventual development into choanoderm with a single layer of choanocytes surrounding the atrium. (F,I) Note that ostia and osculum are not yet formed at day 10. Images were taken with a bright field (A-C), SEM (D-F) or confocal (G-I) microscope. Anti-α-tubulin (green) staining with the nuclei counterstained with DAPI (blue). C, choanocytes; Mo, monaxons; P, pinacocyte; S, sclerocytes; *, external cavity.

juvenile or young syconoid (YS) stages (Fortunato et al., 2014a). For comparative analysis we processed both data sets through similar pipelines, as described in the Materials and Methods section. To assess the global transcriptomic profile underlying PLD and regeneration, we performed principal component analysis (PCA) on individual data sets. We found that both regeneration and PLD follow similar PCA distribution and, surprisingly, the transcriptional changes during regeneration were as variant as PLD (Fig. 5A,B). We also performed hierarchical clustering on both datasets to define the major clusters and identified two major clusters that we classified as early and late stages (Fig. 5C,D). From PCA and hierarchical clustering analysis we observed that clusters in regeneration were organized in a hierarchy consistent with that observed in the PLD.

We then directly compared the transcriptomic variation among regeneration and PLD using PCA. Despite their transcriptomic dynamics, regeneration and PLD fall apart from each other, mainly at PC1 proportion. However, the profiles of regeneration and PLD began to converge as development progressed (Fig. 5E). This indicates that the transcriptomic dynamics of regeneration and PLD are probably similar at advanced stages. Similar conclusions were also drawn from the hierarchical clustering analysis: the late stages (days 10-14, PJUV and JUV) from regeneration were clustered with S5 and PY from PLD (Fig. 5F,G), further suggesting that the later stages of both regeneration and PLD express genes with maximum correlation. High variance among early time points of regenerating and developmental samples indicates that an alternative path was taken during the early stages of regeneration. As noted from the morphology, early stages of regeneration are not strictly a morphological recapitulation of development, with potential for extensive temporal plasticity during early regeneration.

A further comparison was carried out on the significantly differentially expressed genes (*P*adj (FDR)<0.01) at any time point, compared with day1 for regeneration and S1 for PLD. Regeneration exhibited 9097 differentially expressed genes (DEGs), which is comparable to 10,035 DEGs in PLD, suggesting that regeneration

Development (2020) 147, dev193714. doi:10.1242/dev.193714

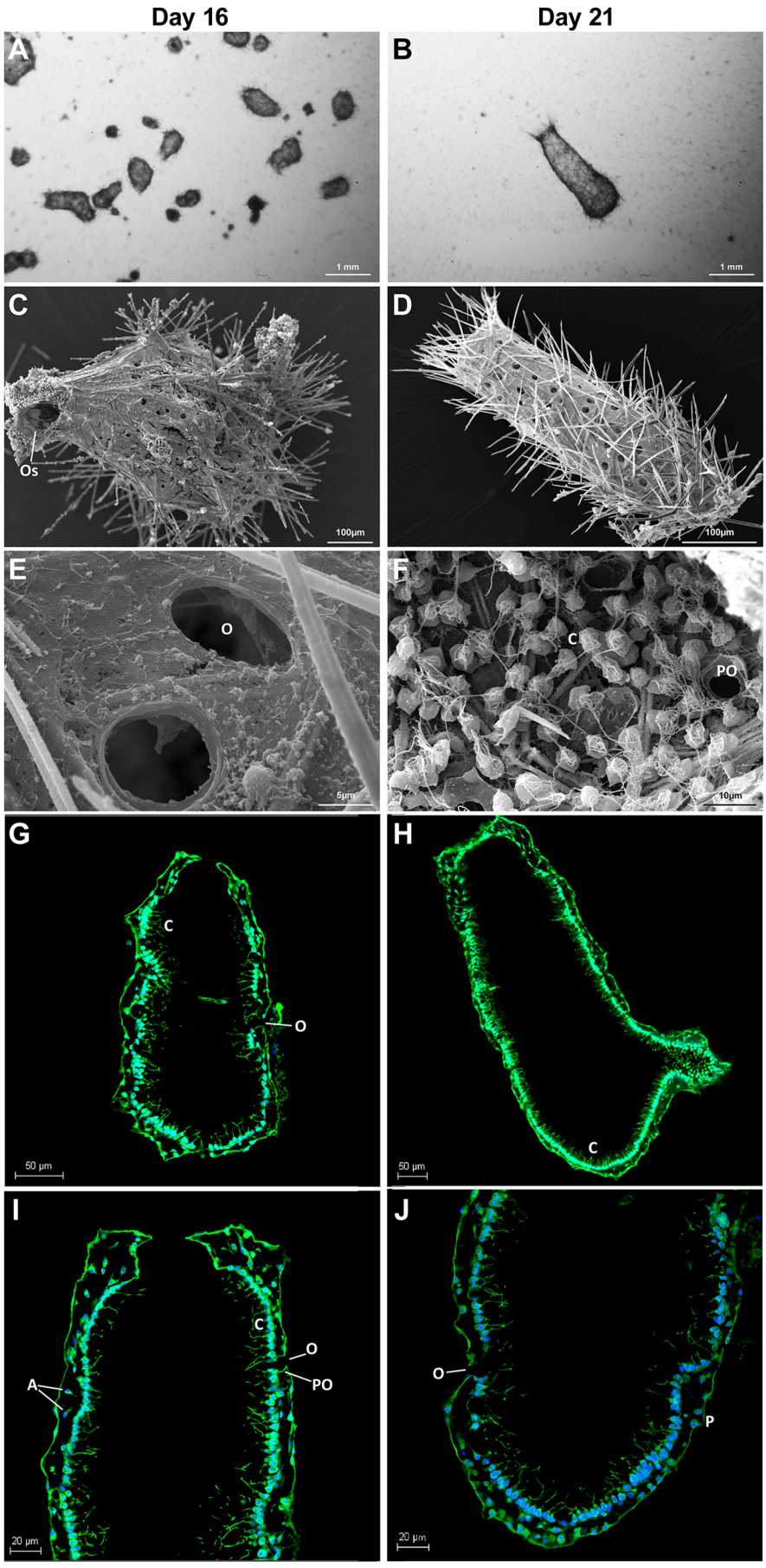

Fig. 4. Development into a functional juvenile. (A,B) General view of pre-juvenile and juvenile stages. (C-J) Osculum opens at apical end and multiple porocytes form ostia. The appearance of ostium and osculum is synchronized (C). Ostia can be seen in the regenerated juvenile (G). A view of ostia from inside shows ostia surrounded by choanocytes (H). Images were taken with a bright field (A,B), SEM (C-F) or confocal (G-J) microscope. Anti-α-tubulin (green) staining with the nuclei counterstained with DAPI (blue). A, archaeocytes or amoebocytes; C, choanocytes; O, Ostia; Os, osculum; P, pinacocyte; PO, porocytes; S, sclerocytes.

Development (2020) 147, dev193714. doi:10.1242/dev.193714

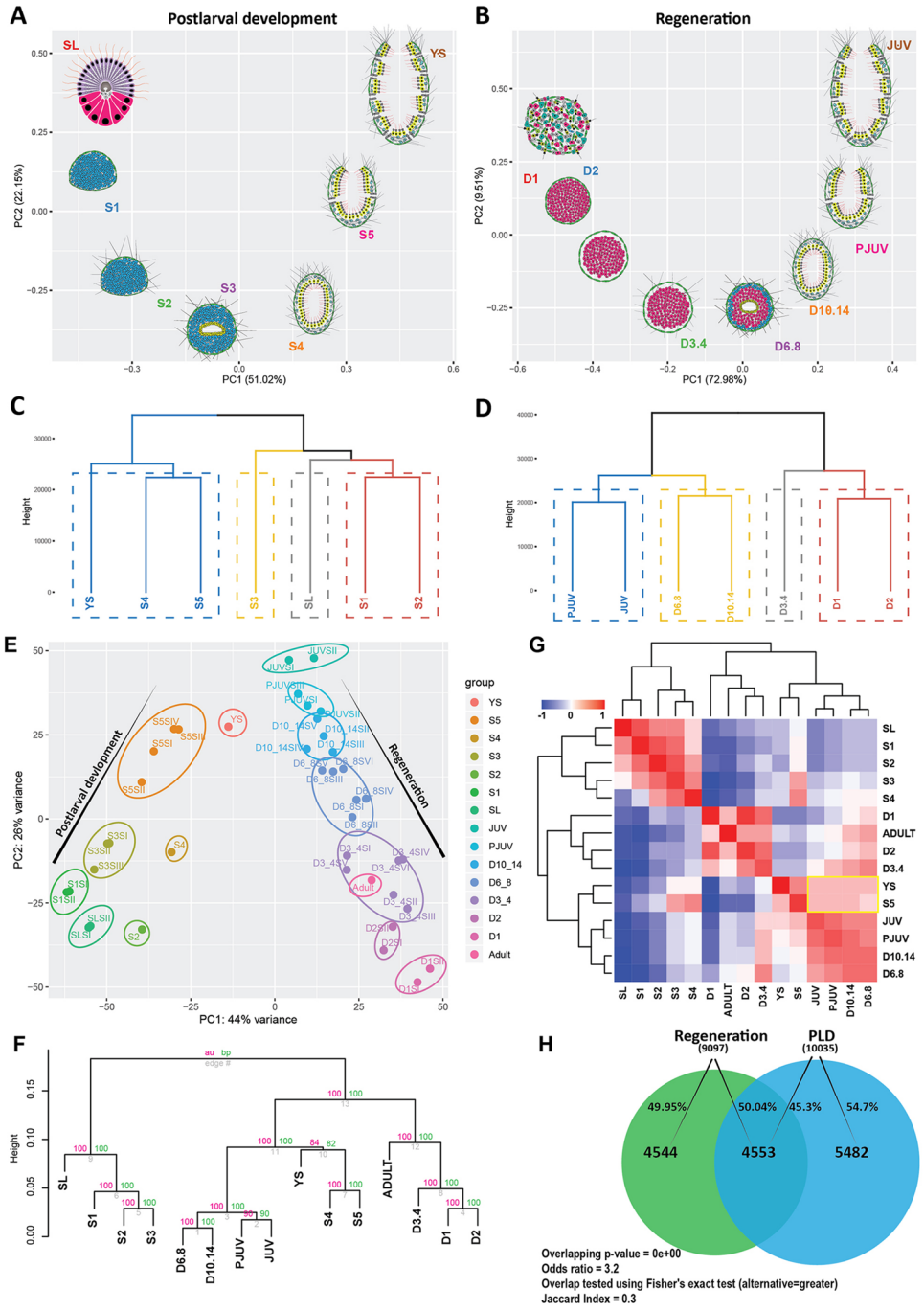

Fig. 5. Overview of postlarval and regeneration transcriptomes. (A) Principal component analysis (PCA) of PLD datasets, showing samples at SL, S1, S2, S3, S4, S5 and YS stages. (B) PCA of regeneration dataset, showing samples at 1, 2, 3-4, 6-8, 10-14, 16-18 (PJUV) and 21-24 (JUV) dpd. (C,D) Hierarchical clustering on PLD (C) and regeneration (D) datasets reveals two major clusters that we classified as early and late stages. This analysis confirmed that clusters in regeneration are organized in a hierarchy consistent with that observed in the PLD. (E) Global transcriptomic comparison of the regeneration and PLD samples. PCA of larval development versus regeneration datasets. Regeneration exhibits similar transcriptomic variation as embryogenesis. The regeneration samples collected at days 10-14, PJUV and JUV stages are close to the S5 and YS stages of PLD. (F) Hierarchical clustering. The dendrogram of both datasets obtained with pvclust is shown with the bootstrap values on each node. There is a significant correlation among late stages of regeneration (days 10-14, PJUV and JUV) with S5 and YS stages of PLD. (G) Comparison of DEGs between PLD and regeneration datasets. The similarity matrix for significantly differentially expressed genes (*P*adj (FDR)<0.01 for any time point comparison against day 1 for regeneration and S1 for PLD). The yellow box highlights the similarity between late stages of regeneration (days 10-14, PJUV and JUV) with S5 and YS stages of PLD. (H) The number of DEGs in regeneration is highly comparable with PLD and ∼50% of genes are commonly expressed. A Fisher's exact test was carried out using the R package GeneOverlap to test the statistical significance between two gene lists. Here, the *P*-value is 0e+00, which means the overlap is highly significant and the odds ratio is much larger than 1, represents a strong association.

exhibits dynamic gene expression equivalent to PLD. Of these dynamically expressed genes, approximately 50% of genes (4553) were commonly expressed in both data sets (Fig. 5H; Table S2), suggesting that half of the PLD genes were deployed during regeneration. As regeneration employs 50% of PLD genes, we intended to compare the expression profiles of these DEGs. We subjected the candidates to Fuzzy c-means clustering (Kumar and Futschik, 2007) to group the genes based on their expression profiles and generated seven clusters for each dataset (Fig. 6A,B; Table S3). After clustering the genes, we analysed the correlation of these clusters among regeneration and PLD by combing all 14 clusters and subjecting them to sample correlation analysis. As observed from the dendrogram, the gene clusters with similar expression patterns between regeneration and PLD probably form a single branch (Fig. 6C). For example, regeneration cluster R6 and PLD cluster D5 were grouped together: notably, these clusters had comparable expression profiles (Fig. 6A,B). Similar results were also reproduced through correlation analysis: the box including R6 and D5 had a relatively high correlation value (Fig. 6D). We found that the majority of the regeneration gene clusters exhibited overlap with specific PLD clusters (Fig. 6C,D), suggesting that regeneration partly resembles PLD by displaying similar gene expression profiles.

Overall, we found that late stages from both regeneration and PLD had a high correlation, thus the major variation in these data is among the early stages. Because regeneration does not start from a zygote or amphiblastula larva, early regeneration stages do not necessarily need to follow a similar pattern of gene expression profile to normal PLD. The early primmorphs were not close to normal swimming larva in

Development (2020) 147, dev193714. doi:10.1242/dev.193714

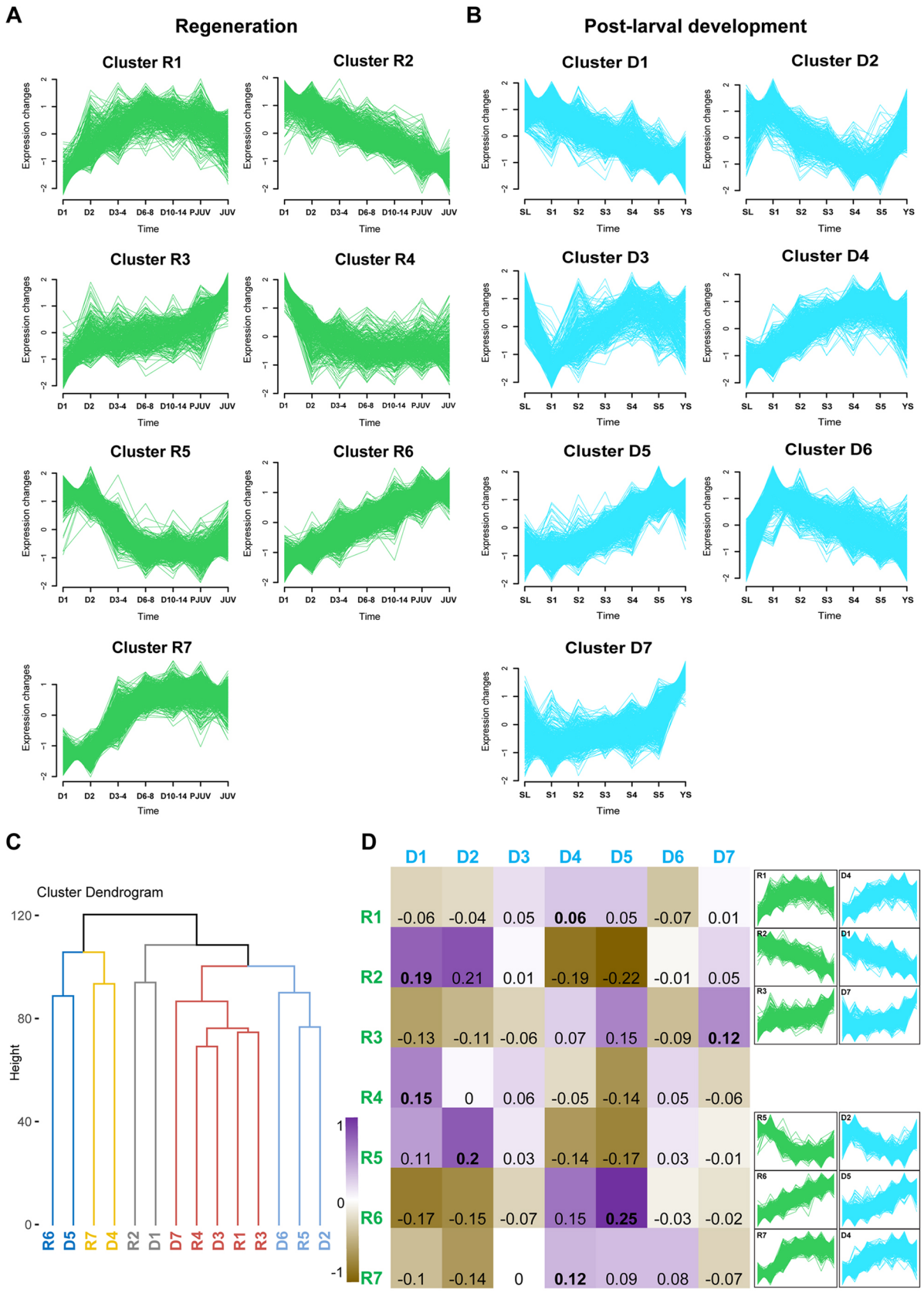

Fig. 6. Regeneration gene clusters overlap with PLD gene clusters. (A,B) A total of 4468 commonly expressed genes between regeneration (A) and PLD (B) were subjected to Fuzzy c-means clustering. Based on their gene expression profiles, we generated seven clusters in both datasets. (C) Hierarchical clustering. The dendrogram of all gene expression clusters from regeneration and PLD. The majority of regeneration gene modules are clustered with PLD gene modules. (D) Cluster overlap table of regeneration versus PLD gene expression clusters produced via Pearson correlation analysis. Bold text indicates the best cluster overlap and their matching gene expression profiles are presented on the right side of the table.

Development (2020) 147, dev193714. doi:10.1242/dev.193714

their gene expression profile; however, the subsequent stages did resemble PLD (Fig. 6). The early primmorphs are unique, as observed from morphological analysis, and multiple cellular events at this stage are expected to have unique gene expression.

Analysis of *S. ciliatum* regeneration gene expression

To the best of our knowledge, sponge regeneration from dissociated somatic cells has not been examined at the transcriptome level. We analysed the regeneration gene expression data to identify developmental and multicellular regulatory genes. We performed a Gene Ontology (GO)-term enrichment analysis to reveal genes associated with various biological processes and molecular function during regeneration. A broad range of eumetazoan developmental regulatory genes were expressed during regeneration; genes such as *Wnt*, *Tgfb*, *Fzd* and *Smad* were differentially expressed (Fig. 7A). Surprisingly, the majority of listed genes were previously identified in *S. ciliatum* during embryonic and postlarval development (Fortunato et al., 2012, 2014a,b; Leininger et al., 2014). From the pathway enrichment analysis, we identified Wnt, TGF-beta, Notch, Hedgehog, FGF and EGF signaling pathways, and the majority of core pathway components were detected (Fig. 7A; Fig. S2, Table S4). Each of these signaling pathways triggers several downstream signaling cascades regulating cell behaviour such as cell-cell and cell-ECM interactions (Sanz-Ezquerro et al., 2017). Along with other biological processes, apoptosis plays an important role during regeneration (Tseng et al., 2007; Pérez-Garijo and Steller, 2015; Warner et al., 2019 preprint). Apoptosis-mediated regeneration permits cell elimination and reorganizes cell composition. Major pathways associated with cell death or apoptosis, including Wnt signaling, the oxidative stress response and the p38 MAPK pathway, were expressed during *S. ciliatum* regeneration (Fig. 7B). Notably, using propidium iodide (PI) staining, we detected cell death in regenerating structures (Fig. 7C), in particular during the early stages. In fact, in our current analysis of *S. ciliatum* regeneration gene expression (Fig. 7B), we found a high expression of apoptotic genes at early stages, emphasizing the role of apoptosis in remodelling the primmorphs to initiate re-development. This coincides with a recent study in *Nematostella vectensis* showing at the functional level that apoptosis is required for the initiation of regeneration (Warner et al., 2019 preprint).

After tissue dissociation, the initial cellular source constitutes a heterogeneous pool of adult somatic cells. During the initial regeneration phase (days 1-3), the dissociated cells re-aggregate and organize into a morphologically distinguishable structure (Fig. 2). During the development of multicellular organisms, cells change their position extensively and this process is governed by cell-adhesion and motility molecules. Similarly, sponge regeneration is guided through a series of cellular events, including initial cell aggregation and followed by cell organization. Hence, we analysed the genes associated with cell adhesion and cell mobility molecules. Using GO term analysis of DEGs, we identified members associated with cell-adhesion gene families, including those that encode cell-surface receptors, cytoplasmic linkers and ECM proteins (Fig. 8A,B). Expression of these cell-cell and cell-ECM adhesions signify highly integrated networks that are crucial in enabling individual cells to adhere and organize into a multicellular structure (Weber et al., 2011).

Cadherins mediate cell-cell adhesion, broadly regulating morphological aspects during development (Peyriéras et al., 1983; Nichols et al., 2006). Several genes associated with the cadherin pathway were significantly differentially expressed (Fig. 8B). Along with cadherins, we also identified genes associated with the integrin pathway. Cell migration is a process that is highly dependent on adhesion and junction molecules such as integrins (Friedl, 2004; Friedl et al., 1998). The co-expression of cadherin, integrins and other downstream scaffolding and adaptor proteins such as RhoGTPases, tyrosine kinases and phosphatases suggests that together these molecules contribute to initiation of the early events of regeneration. Integrins mediate contact between cells and ECM in many organisms by binding to ECM proteins (Campbell and Humphries, 2011; Humphries et al., 2006; Theocharis et al., 2016; Seebeck et al., 2017; Daley et al., 2008). Three major ECM structural proteins (fibronectin, collagen and laminin) displayed differential expression (Fig. 8A), demonstrating the importance of ECM molecules during regeneration. In summary, our analysis indicates that the initial phases of regeneration, including cell aggregation and organization, are guided by a set of molecules associated with cell-cell and cell-ECM adhesion.

Lessons to learn on the origin of multicellularity from the sponge regeneration model

The current hypothesis on the origin of multicellular animals generally agrees that choanoflagellates share a common ancestor with animals (Fig. 8). This idea is based on the molecular phylogeny and morphological similarity between choanoflagellates and sponge choanocytes (Fig. 8C-E) (Laundon et al., 2019; Adamska, 2016; Nielsen, 2008; Brunet et al., 2019; King et al., 2008; Shalchian-Tabrizi et al., 2008). Study of the early regeneration events in sponge, including the signalling molecules triggering the aggregation of cells, can provide a window into understanding the transition from unicellular to multicellular life forms. Recent studies of multiple unicellular holozoans such as choanoflagellates have revealed several genes related to multicellularity, including cell differentiation, cell-cell adhesion and cell-ECM adhesion (Fig. 8F) (Hehenberger et al., 2017; Sogabe et al., 2019; Suga et al., 2013; King et al., 2003), suggesting that these factors evolved before the origin of multicellular animals. Indeed, our current analysis of *S. ciliatum* regeneration gene expression found that several cell signalling and adhesion protein families, including cadherin, integrins and ECM molecules, were highly expressed within 24 h of dissociation and are probably involved in cell aggregation and further regeneration processes (Fig. 8A,B). The main focus of the current study was to test the homology between regeneration and development; hence, sampling was prioritized according to morphology, with the first sample collected 24 h after dissociation. To gain an in-depth understanding of the initial signalling cascades triggering aggregation, tight sampling during the initial aggregation stages would be beneficial. Future studies in this direction will provide further insights into the evolutionary mechanisms underlying the origin of multicellular animals.

Conclusions

Sponge regeneration is a powerful system for understanding the cellular and molecular mechanisms governing animal regeneration in general. This is crucial for understanding the evolution of multicellularity. We compared regeneration and postembryonic development in *S. ciliatum* by applying both morphological and RNA-seq analyses to reveal the correlation between these phenomena. Here, we demonstrate that *S. ciliatum* regeneration is governed by core components of the Wnt, Tgfβ, Notch and Hedgehog signaling pathways, which are known to guide various aspects of embryonic development and morphogenesis in extant eumetazoans. Furthermore, we have identified major eumetazoan cell-adhesion gene families, including those that encode cell-surface receptors, cytoplasmic linkers and ECM proteins. We found that approximately 50% of genes differentially expressed

Development (2020) 147, dev193714. doi:10.1242/dev.193714

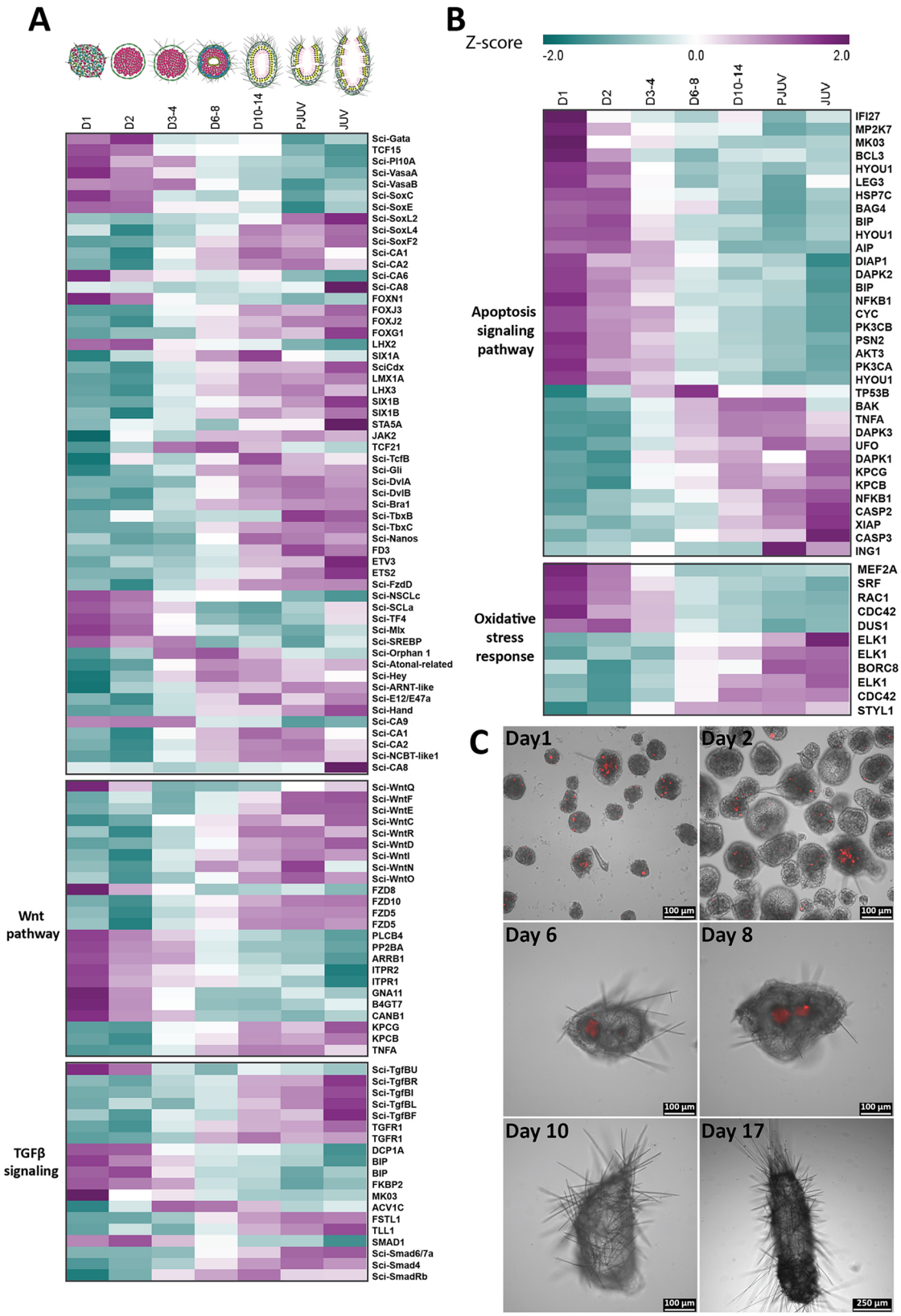

Fig. 7. Gene expression across *S. ciliatum* regeneration. (A) Heatmap of significantly differentially expressed genes, displaying a selected list of transcriptional factors and Wnt and Tgfb pathways genes. Most of the listed genes are known to associate with a range of eumetazoan developmental regulatory pathways and have been previously identified in *S. ciliatum* embryonic development. (B) Heatmap showing the relative expression of genes associated with cell death (apoptosis signaling pathway and response to oxidative stress). Note the large changes in gene expression at day 1 and the gradual decrease in expression later. Heatmaps show scaled expression (row z-score) of integrins with significantly different expression [*P*adj (FDR)<0.01 for any time point comparison against day 1]. (C) Cell death is detected in regenerating structures. The regenerating structures were stained with PI to observe apoptotic cell death during regeneration.

Development (2020) 147, dev193714. doi:10.1242/dev.193714

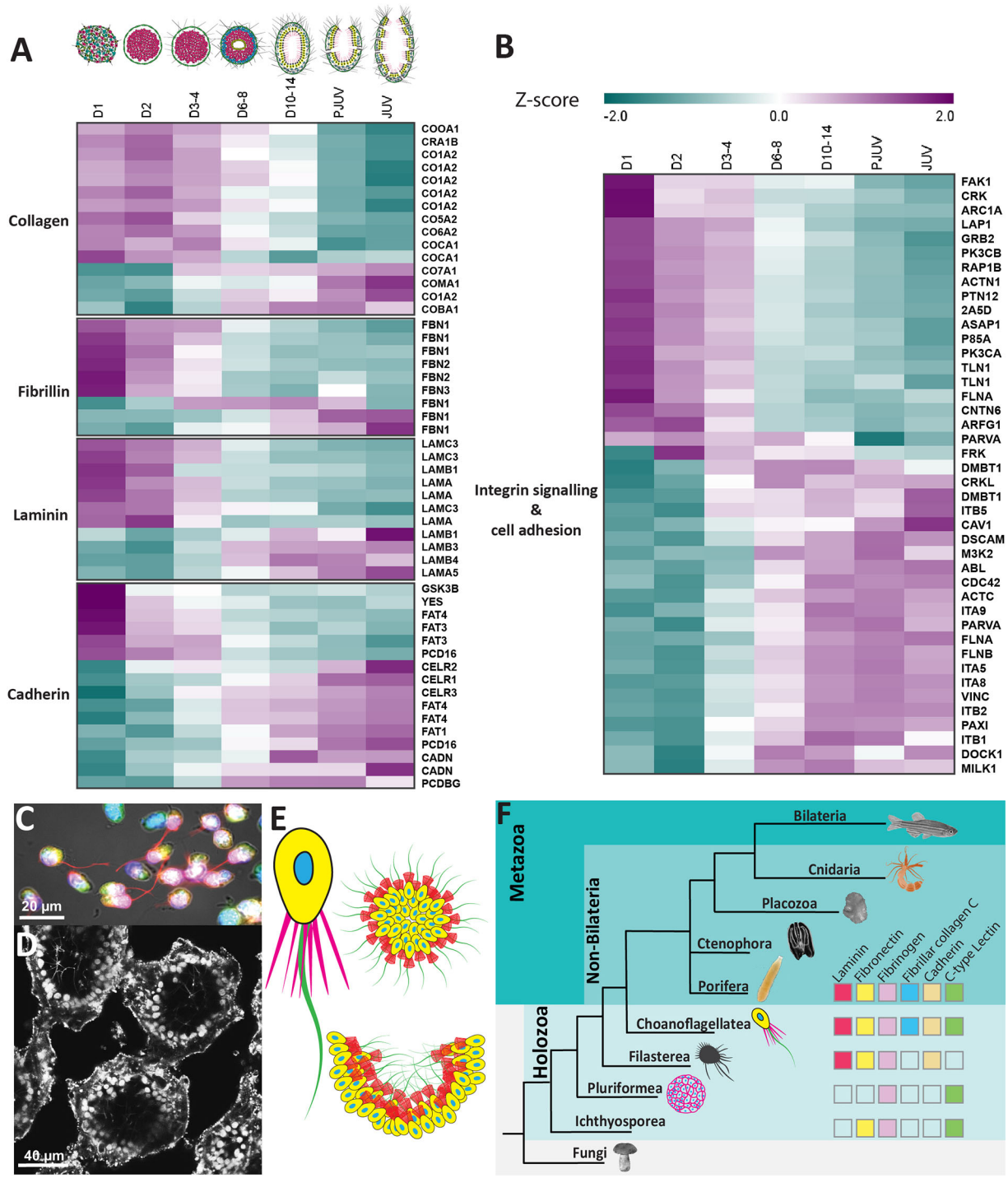

Fig. 8. The origin of animal multicellularity. (A,B) Heatmap showing relative expression of ECM and cell adhesion and motility (integrin, cadherin and scaffold) genes. A broad range of genes start expressing within 24 hpd, and are possibly involved in cell aggregation, adhesion and motility during regeneration. (C-E) Morphological similarities between choanocytes and choanoflagellates: *S. ciliatum* choanocytes among dissociated cells (C) and choanocyte chambers of sponge *S. ciliatum* (D) compared with unicellular and multicellular (colonial) forms of choanoflagellates (E). (F) Phylogenetic tree presenting animals and closely related unicellular holozoan lineages. The position of Ctenophora and Porifera is indicated as a polytomy because of current uncertainty about their evolutionary origin. The boxes indicate animal ECM and cell-adhesion family proteins found in unicellular holozoan lineages; empty boxes indicate absence.

during postlarval development are also expressed in regeneration. The *S. ciliatum* dissociated cells thus deploy a set of genes similar to those deployed during embryonic and larval development to assist regeneration. This has important implications for use of the *S. ciliatum* regeneration system to model the evolution of multicellularity. In this study, our sampling was aimed at dissecting the early cellular events in regeneration; additional high throughput studies over multiple time points can address deeper questions such as somatic cell trajectory during regeneration.

Development (2020) 147, dev193714. doi:10.1242/dev.193714

MATERIALS AND METHODS

Animal collection and regeneration protocol

Adult *S. ciliatum* specimens were collected in the vicinity of Plymouth, Devon, UK. All specimens were at the stage of post reproduction growth and did not contain any reproductive elements. Prior to experimentation, animals were maintained in the aquarium with filtered seawater (FSW) for no longer than 2-4 h. Each *S. ciliatum* was cut into small pieces using a scalpel and microscissors, then mechanically passed through 40 µm nylon mesh (Fisherbrand) into a petri dish (35 mm). The dissociated cells were suspended in FSW and pipetted multiple times to allow maximum dissociation. The dissociated cells from each individual were distributed into six-well plates. The number of cells in the plates ranged from 1.2×10^6 to 1.5×10^7. The dissociated cells were maintained at 15°C in the dark. Every 24 h the culture medium was exchanged with FSW and bright-field images were collected daily. Initially, when attempting to follow published protocols (Wilson, 1907; Huxley, 1921; Korotkova, 1972), we were unsuccessful with *S. ciliatum* regeneration as the majority of cell aggregates were unable to progress to functional juveniles. Hence, we modified the protocol by fractionating the dissociated cells using centrifugation. We followed similar instructions until cell dissociation, and then we centrifuged the dissociated cells at 1.2 rpm for 2 min. The supernatant was collected into a new 1.5 ml tube and re-centrifuged at 2.5 rpm for 2 min. The cell pellets from both steps were suspended in FSW and distributed individually in six-well plates. The cells pelleted at 2.5 rpm have a high regeneration ability in comparison to the cells pelleted at 1.2 rpm. In the current study, we used the aggregates collected from 2.5 rpm wells. Apart from standardizing the protocol, the regeneration experiment was performed seven times independently and 8-12 specimens were used in each experiment. For morphological analysis, the samples were collected at 1, 2, 3, 4, 5, 6, 8, 10, 12, 14, 18, 21 and 24 dpd, with 10-20 regenerative structures per replicate.

Whole-mount immunofluorescence

The specimens were fixed for 1 h at 4°C on a roller with 0.05% glutaraldehyde and 4% paraformaldehyde (PFA) in PBS buffer. After fixation, the samples were washed five times with PBST [1× PBS, 0.05% (vol/vol) Tween-20] for 5 min. For long term storage, the specimens were dehydrated in a series of ethanol dilutions and stored in 70% ethanol at 4°C. For whole-mount immunofluorescence, the samples were permeabilized in Dent's fixative (80% methanol, 20% DMSO) for 15 min and followed by rehydration through series of methanol dilutions (70, 50 and 25% methanol) for 5 min per dilution. The samples were washed with PBST for 3×10 min, then blocked in 5% BSA in PBST for 1 h at room temperature. Primary antibody (1:500 dilution, mouse anti-α-tubulin; cat #T9026, Sigma-Aldrich) incubation was performed in a blocking solution (1% BSA in PBST) for 24-36 h at 4°C. The samples were washed with PBST for 5×5 min, after which samples were incubated with secondary antibodies (1:250 dilution; goat anti-mouse IgG Alexa Fluor 594; cat #A-11032, Thermo Fisher Scientific) diluted in blocking solution overnight at 4°C. Then, the samples were washed with PBST for 5×10 min and clarified following iDISCO protocol (Renier et al., 2014). Imaging was performed on Leica TCS SP8 DLS and Leica DMi8 confocal microscopes.

Fixation of regenerating specimens for scanning electron microscopy

The specimens were fixed overnight at 4°C with 2.5% glutaraldehyde in PBS buffer, then rinsed three times with PBS buffer for 10 min. The specimens were postfixed in 1% osmium tetroxide in PBS buffer at room temperature. After post-fixation, the specimens were dehydrated in a series of ethanol dilutions until 100% ethanol and absolute ethanol was gradually exchanged with hexamethyldisilazane (HMDS). After the final 100% HMDS solution step, the specimens were left in a fume hood overnight to allow the HMDS to evaporate. After overnight drying, the samples were mounted on aluminium stabs and coated with gold. SEM imaging was done using a JEOL 6610 LV microscope.

RNA sequencing and differential gene expression

Regeneration is semi-synchronous among individuals, even though the variation is mild (generally varies ±1 day). Keeping this in mind, we collected the regenerating samples principally based on morphological signatures, apart from the samples on days 1 and 2 after dissociation. For RNA isolation, the early regenerating samples were collected at days 1 and 2. For later stages, the samples were primarily collected based on the morphological state extending between days 3-4, 6-8, 10-14, 16-18 (PJUV) and 21-24 (JUV) post dissociation. Each sample was pooled from a minimum of three individuals and also included samples from different batches, as detailed in Table S1 (first column). The samples were carefully collected using a pipette and excess medium was removed before snap freezing in liquid nitrogen and storing at −80°C until further processing. Due to the small size of primmorphs at early stages (1 and 2 dpd), samples collected from multiple biological replicates were combined to acquire an adequate amount of RNA for sequencing. For the later stages, only three biological replicates were combined into one sample during RNA isolation. Total RNA was isolated using TRI Reagent according to the manufacturer's protocol. RNA quality was assessed using Agilent RNA 6000 Nano Kit on the Agilent 2100 Bioanalyzer (Agilent, USA), and only samples with RNA integrity number (RIN) ≥8.0 were considered for sequencing. Sample library preparation for RNA sequencing was accomplished using the SENSE mRNA-Seq Library Prep Kit (Lexogen). Before sequencing, the libraries were pre-assessed using the Agilent High Sensitivity DNA Kit (Agilent, USA) and quantified using Qubit 1× dsDNA HS Assay Kit (Invitrogen). The sequencing was outsourced (GENEWIZ Illumina NovaSeq/HiSeq 2×150 bp sequencing), generating 20 million paired-end reads per replicate. Raw data was deposited at NCBI GEO submission GSE149471. After de-multiplexing and filtering high-quality sequencing reads, the adapter contamination was removed by using Trimmomatic v0.36 (Bolger et al., 2014). The quality of the reads was verified using FastQC (Andrews, 2010). The *S. ciliatum* genome was sourced from Dryad (https://datadryad.org/stash/dataset/doi:10.5061/dryad.tn0f3) (Fortunato et al., 2014a). Processed reads from each sample were mapped to the *S. ciliatum* genome using HISAT2 (Kim et al., 2019). Next, the mapped reads were passed to StringTie (Pertea et al., 2015) for transcript assembly. After initial assembly, all assembled transcripts from regeneration and development were merged using the merge module in StringTie (assembled contigs; https://doi.org/10.17031/1669), which merges all the gene structures found in any of the samples. The BAM file and GFT file generated by the merge (Table S2) were fed into featureCounts (Liao et al., 2014) to extract the reads counts per transcript. Differential expression analyses were performed using DESeq2 (Galaxy Version 2.11.40.6) (Love et al., 2014). The PCA, hierarchical clustering and heatmaps were generated using the R package in R-studio (version 1.2.5019). For functional annotation, the transcripts were extracted from the GTF annotation file using the gffread utility and the LongOrfs were acquired using TransDecoder. We used blastp (Altschul et al., 1997) with the default curated gathering threshold to predict the protein orthologues against the Uniprot database. The GO term enrichment was performed using gene annotation tools including the PANTHER Classification System (Mi et al., 2012) and DAVID (Huang et al., 2009).

Detection of cell death

Regenerating structures were transferred into a glass-bottom dish and stained with PI at a concentration of 10 µg/ml in FSW. After 30 min of incubation, the staining medium was replaced with fresh FSW before fluorescence microscopy. The analysis was performed on regenerating structures collected from four individual animals. The samples were collected at 1, 2, 6, 8, 10, 13, 14 and 17 dpd, with ten regenerative structures collected per replicate.

Acknowledgements

The authors thank John Bishop and Christine Wood for their support in acquiring *S. ciliatum* specimens. We thank Glenn Harper and the team at the Plymouth Electron Microscopy Lab for their assistance during the imaging. We thank Ro Allen for his help with R statistics.

Competing interests

The authors declare no competing or financial interests.

Author contributions

Conceptualization: A.S., V.M.; Methodology: A.S., E.G.R., Y.T., V.M.; Software: N.C.; Validation: A.S., E.G.R., V.M.; Formal analysis: A.S., Y.T., N.C., V.M.; Investigation: A.S., V.M.; Data curation: A.S., E.G.R., V.M.; Writing - original draft: V.M.; Writing - review & editing: A.S., E.G.R., Y.T., N.C.; Visualization: A.S., E.G.R., Y.T., V.M.; Supervision: V.M.

Funding

This work was supported by the Anne Warner endowed Fellowship through the Marine Biological Association of the UK.

Data availability

Bulk RNA sequencing data have been deposited GEO under accession number GSE149471.

Supplementary information

Supplementary information available online at
https://dev.biologists.org/lookup/doi/10.1242/dev.193714.supplemental

Peer review history

The peer review history is available online at
https://dev.biologists.org/lookup/doi/10.1242/dev.193714.reviewer-comments.pdf

References

Adamska, M. (2016). Sponges as models to study emergence of complex animals. *Curr. Opin. Genet. Dev.* **39**, 21-28. doi:10.1016/j.gde.2016.05.026

Adamska, M. (2018). Differentiation and transdifferentiation of sponge cells. In *Marine Organisms as Model Systems in Biology and Medicine* (ed. M. Kloc and J. Z. Kubiak), pp. 229-253. Cham: Springer International Publishing.

Altschul, S. F., Madden, T. L., Schäffer, A. A., Zhang, J., Zhang, Z., Miller, W. and Lipman, D. J. (1997). Gapped BLAST and PSI-BLAST: a new generation of protein database search programs. *Nucleic Acids Res.* **25**, 3389-3402. doi:10.1093/nar/25.17.3389

Amiel, A. R., Johnston, H., Nedoncelle, K., Warner, J., Ferreira, S. and Röttinger, E. (2015). Characterization of morphological and cellular events underlying oral regeneration in the sea anemone, Nematostella vectensis. *Int. J. Mol. Sci.* **16**, 28449-28471. doi:10.3390/ijms161226100

Andrews, S. (2010). FastQC: a quality control tool for high throughput sequence data. http://www.bioinformatics.babraham.ac.uk/projects/fastqc.

Bolger, A. M., Lohse, M. and Usadel, B. (2014). Trimmomatic: a flexible trimmer for Illumina sequence data. *Bioinformatics* **30**, 2114-2120. doi:10.1093/bioinformatics/btu170

Brunet, T. and King, N. (2017). The origin of animal multicellularity and cell differentiation. *Dev. Cell* **43**, 124-140. doi:10.1016/j.devcel.2017.09.016

Brunet, T., Larson, B. T., Linden, T. A., Vermeij, M. J. A., McDonald, K. and King, N. (2019). Light-regulated collective contractility in a multicellular choanoflagellate. *Science* **366**, 326-334. doi:10.1126/science.aay2346

Bryant, D. M., Johnson, K., DiTommaso, T., Tickle, T., Couger, M. B., Payzin-Dogru, D., Lee, T. J., Leigh, N. D., Kuo, T.-H., Davis, F. G. et al. (2017). A tissue-mapped axolotl de novo transcriptome enables identification of limb regeneration factors. *Cell Rep.* **18**, 762-776. doi:10.1016/j.celrep.2016.12.063

Burton, P. M. and Finnerty, J. R. (2009). Conserved and novel gene expression between regeneration and asexual fission in Nematostella vectensis. *Dev. Genes Evol.* **219**, 79-87. doi:10.1007/s00427-009-0271-2

Campbell, I. D. and Humphries, M. J. (2011). Integrin structure, activation, and interactions. *Cold Spring Harbor Perspect. Biol.* **3**, a004994. doi:10.1101/cshperspect.a004994

Daley, W. P., Peters, S. B. and Larsen, M. (2008). Extracellular matrix dynamics in development and regenerative medicine. *J. Cell Sci.* **121**, 255-264. doi:10.1242/jcs.006064

Eerkes-Medrano, D. I. and Leys, S. P. (2006). Ultrastructure and embryonic development of a syconoid calcareous sponge. *Invertebr. Biol.* **125**, 177-194. doi:10.1111/j.1744-7410.2006.00051.x

Ereskovsky, A. V. (2010). Development of sponges from the Class Calcarea Bowerbank, 1864. In *The Comparative Embryology of Sponges*, pp. 3-36. Dordrecht: Springer Netherlands.

Fortunato, S., Adamski, M., Bergum, B., Guder, C., Jordal, S., Leininger, S., Zwafink, C., Rapp, H. and Adamska, M. (2012). Genome-wide analysis of the sox family in the calcareous sponge Sycon ciliatum: multiple genes with unique expression patterns. *EvoDevo* **3**, 14. doi:10.1186/2041-9139-3-14

Fortunato, S. A. V., Adamski, M., Ramos, O. M., Leininger, S., Liu, J., Ferrier, D. E. K. and Adamska, M. (2014a). Calcisponges have a ParaHox gene and dynamic expression of dispersed NK homeobox genes. *Nature.* **514**, 620-623. doi:10.1038/nature13881

Fortunato, S. A. V., Leininger, S. and Adamska, M. (2014b). Evolution of the Pax-Six-Eya-Dach network: the calcisponge case study. *EvoDevo* **5**, 23. doi:10.1186/2041-9139-5-23

Franzen, W. (1988). Oogenesis and larval development of Scypha ciliata (Porifera, Calcarea). *Zoomorphology* **107**, 349-357. doi:10.1007/BF00312218

Friedl, P. (2004). Prespecification and plasticity: shifting mechanisms of cell migration. *Curr. Opin. Cell Biol.* **16**, 14-23. doi:10.1016/j.ceb.2003.11.001

Friedl, P., Zänker, K. S. and Bröcker, E.-B. (1998). Cell migration strategies in 3-D extracellular matrix: differences in morphology, cell matrix interactions, and integrin function. *Microsc. Res. Tech.* **43**, 369-378. doi:10.1002/(SICI)1097-0029(19981201)43:5<369::AID-JEMT3>3.0.CO;2-6

Haeckel, E. (1874). Die Gastrae Theorie, die phylogenetische Classification des Thierreichs und die Homologie der Keimblatter. *Jena Zeitsch Naturwiss* **8**, 1-55.

Hehenberger, E., Tikhonenkov, D. V., Kolisko, M., del Campo, J., Esaulov, A. S., Mylnikov, A. P. and Keeling, P. J. (2017). Novel predators reshape holozoan phylogeny and reveal the presence of a two-component signaling system in the ancestor of animals. *Curr. Biol.* **27**, 2043-2050.e6. doi:10.1016/j.cub.2017.06.006

Huang, D. W., Sherman, B. T. and Lempicki, R. A. (2009). Bioinformatics enrichment tools: paths toward the comprehensive functional analysis of large gene lists. *Nucleic Acids Res.* **37**, 1-13. doi:10.1093/nar/gkn923

Humphries, J. D., Byron, A. and Humphries, M. J. (2006). Integrin ligands at a glance. *J. Cell Sci.* **119**, 3901-3903. doi:10.1242/jcs.03098

Huxley, J. S. (1921). Memoirs: further studies on restitution-bodies and free tissue-culture in Sycon. *Q. J. Microsc. Sci.* **s2-65**, 293-322.

Huxley, J. S. and Bourne, G. C. (1911). Some phenomena of regeneration in sycon: with a note on the structure of its collar-cells. *Philos. Trans. R. Soc. Lond. B Contain. Papers Biol. Character* **202**, 165-189.

Kim, D., Paggi, J. M., Park, C., Bennett, C. and Salzberg, S. L. (2019). Graph-based genome alignment and genotyping with HISAT2 and HISAT-genotype. *Nat. Biotechnol.* **37**, 907-915. doi:10.1038/s41587-019-0201-4

King, N., Hittinger, C. T. and Carroll, S. B. (2003). Evolution of key cell signaling and adhesion protein families predates animal origins. *Science* **301**, 361-363. doi:10.1126/science.1083853

King, N., Westbrook, M. J., Young, S. L., Kuo, A., Abedin, M., Chapman, J., Fairclough, S., Hellsten, U., Isogai, Y., Letunic, I. et al. (2008). The genome of the choanoflagellate Monosiga brevicollis and the origin of metazoans. *Nature* **451**, 783-788. doi:10.1038/nature06617

Korotkova, G. P. (1970). Regeneration and somatic embryogenesis in sponges. In: *The Biology of the Porifera. Zoological Society of London* (ed. W. G. Fry), pp 423-436. Academic Press.

Korotkova, G. (1972). *Comparative morphological investigations of development of sponges from dissociated cells*. Transactions of Leningrad Society of Naturalists. **78**, 74-109.

Kumar, L. and Futschik, M. E. (2007). Mfuzz: a software package for soft clustering of microarray data. *Bioinformation* **2**, 5-7. doi:10.6026/97320630002005

Laundon, D., Larson, B. T., McDonald, K., King, N. and Burkhardt, P. (2019). The architecture of cell differentiation in choanoflagellates and sponge choanocytes. *PLoS Biol.* **17**, e3000226. doi:10.1371/journal.pbio.3000226

Leininger, S., Adamski, M., Bergum, B., Guder, C., Liu, J., Laplante, M., Bråte, J., Hoffmann, F., Fortunato, S., Jordal, S. et al. (2014). Developmental gene expression provides clues to relationships between sponge and eumetazoan body plans. *Nat. Commun.* **5**, 3905. doi:10.1038/ncomms4905

Liao, Y., Smyth, G. K. and Shi, W. (2014). featureCounts: an efficient general purpose program for assigning sequence reads to genomic features. *Bioinformatics* **30**, 923-930. doi:10.1093/bioinformatics/btt656

Love, M. I., Huber, W. and Anders, S. (2014). Moderated estimation of fold change and dispersion for RNA-seq data with DESeq2. *Genome Biol.* **15**, 550. doi:10.1186/s13059-014-0550-8

Mi, H., Muruganujan, A. and Thomas, P. D. (2012). PANTHER in 2013: modeling the evolution of gene function, and other gene attributes, in the context of phylogenetic trees. *Nucleic Acids Res.* **41**, D377-D386. doi:10.1093/nar/gks1118

Nichols, S. A., Dirks, W., Pearse, J. S. and King, N. (2006). Early evolution of animal cell signaling and adhesion genes. *Proc. Natl Acad. Sci. USA* **103**, 12451-12456. doi:10.1073/pnas.0604065103

Nielsen, C. (2008). Six major steps in animal evolution: are we derived sponge larvae? *Evol. Dev.* **10**, 241-257. doi:10.1111/j.1525-142X.2008.00231.x

Onai, T., Matsuo-Takasaki, M., Inomata, H., Aramaki, T., Matsumura, M., Yakura, R., Sasai, N. and Sasai, Y. (2007). XTsh3 is an essential enhancing factor of canonical Wnt signaling in Xenopus axial determination. *EMBO J.* **26**, 2350-2360. doi:10.1038/sj.emboj.7601684

Pérez-Garijo, A. and Steller, H. (2015). Spreading the word: non-autonomous effects of apoptosis during development, regeneration and disease. *Development* **142**, 3253-3262. doi:10.1242/dev.127878

Pertea, M., Pertea, G. M., Antonescu, C. M., Chang, T.-C., Mendell, J. T. and Salzberg, S. L. (2015). StringTie enables improved reconstruction of a transcriptome from RNA-seq reads. *Nat. Biotechnol.* **33**, 290-295. doi:10.1038/nbt.3122

Peyriéras, N., Hyafil, F., Louvard, D., Ploegh, H. L. and Jacob, F. (1983). Uvomorulin: a nonintegral membrane protein of early mouse embryo. *Proc. Natl Acad. Sci. USA* **80**, 6274-6277. doi:10.1073/pnas.80.20.6274

Renier, N., Wu, Z., Simon, D. J., Yang, J., Ariel, P. and Tessier-Lavigne, M. (2014). iDISCO: a simple, rapid method to immunolabel large tissue samples for volume imaging. *Cell* **159**, 896-910. doi:10.1016/j.cell.2014.10.010

Sanz-Ezquerro, J. J., Munsterberg, A. E. and Stricker, S. (2017). Editorial: signaling pathways in embryonic development. *Front. Cell Dev. Biol.* **5**, a76. doi:10.3389/fcell.2017.00076

Seebeck, F., März, M., Meyer, A.-W., Reuter, H., Vogg, M. C., Stehling, M., Mildner, K., Zeuschner, D., Rabert, F. and Bartscherer, K. (2017). Integrins are required for tissue organization and restriction of neurogenesis in regenerating planarians. *Development* **144**, 795-807. doi:10.1242/dev.139774

Shalchian-Tabrizi, K., Minge, M. A., Espelund, M., Orr, R., Ruden, T., Jakobsen, K. S., Cavalier-Smith, T. and Aramayo, R. (2008). Multigene phylogeny of choanozoa and the origin of animals. *PLoS ONE* **3**, e2098. doi:10.1371/journal.pone.0002098

Sogabe, S., Hatleberg, W. L., Kocot, K. M., Say, T. E., Stoupin, D., Roper, K. E., Fernandez-Valverde, S. L., Degnan, S. M. and Degnan, B. M. (2019). Pluripotency and the origin of animal multicellularity. *Nature* **570**, 519-522. doi:10.1038/s41586-019-1290-4

Suga, H., Chen, Z., de Mendoza, A., Sebé-Pedrós, A., Brown, M. W., Kramer, E., Carr, M., Kerner, P., Vervoort, M., Sánchez-Pons, N. et al. (2013). The Capsaspora genome reveals a complex unicellular prehistory of animals. *Nat. Commun.* **4**, 2325. doi:10.1038/ncomms3325

Theocharis, A. D., Skandalis, S. S., Gialeli, C. and Karamanos, N. K. (2016). Extracellular matrix structure. *Adv. Drug Delivery. Rev.* **97**, 4-27. doi:10.1016/j.addr.2015.11.001

Tseng, A.-S., Adams, D. S., Qiu, D., Koustubhan, P. and Levin, M. (2007). Apoptosis is required during early stages of tail regeneration in Xenopus laevis. *Dev. Biol.* **301**, 62-69. doi:10.1016/j.ydbio.2006.10.048

Warner, J. F., Amiel, A. R., Johnston, H. and Rottinger, E. (2019). Regeneration is a partial redeployment of the embryonic gene network. *bioRxiv*, 658930. doi:10.1101/658930

Weber, G. F., Bjerke, M. A. and DeSimone, D. W. (2011). Integrins and cadherins join forces to form adhesive networks. *J. Cell Sci.* **124**, 1183-1193. doi:10.1242/jcs.064618

Wilson, H. V. (1907). On some phenomena of coalescence and regeneration in sponges. *J. Exp. Zool.* **5**, 245-258. doi:10.1002/jez.1400050204